2.8 ENTRAINMENT AND THE FINE STRUCTURE OF THE STRATOCUMULUS TOPPED BOUNDARY LAYERS

Q. Wang[1], M. S. Horner[1], S. Wang[2], and J.A. Kalogiros[3]

[1]Naval Postgraduate School, Monterey, CA
[2]Naval Research Lab, Monterey, CA
[3]National Observatory of Athens, Athens, Greece

1. INTRODUCTION

It has been recognized that entrainment is one of the most important processes that affecting the evolution of marine stratocumulus cloud. However, many questions remain on the fine structure of the stratocumulus cloud top at which entrainment occurs. Early studies of Nichols and Turton (1986) and others showed the strong variation at the vicinity of the cloud top from measurements by research aircraft flying at a constant level near the cloud top. The abrupt change in temperature and water vapor at the boundaries of the cloud penetrations appeared to indicate a sharp transition of these variables across the cloud top. In a more recent study, Lenschow et al. (2000) applied a composite technique to analyze the variation of thermodynamic variable using similar measurements near the cloud top. Their analyses found a near discontinuity occurring in temperature and water vapor across the cloud top over an equivalent vertical distance of 0.3 m and hence again reveal the sharp transition at the cloud top. These studies seem to be consistent with the classical view of the stratocumulus cloud top where a sharp inversion collocates with the cloud top.

Recently, Moeng et al. (2005) found in large eddy simulations (LES) that this view does not appear to hold. Their LES simulations showed that sometimes the cloud layer is below the main temperature inversion. Here we intend to explore the cloud top structure in fine detail using in situ observations by a research aircraft, the Electra operated by the National Center for Atmospheric Research (NCAR) during the Atlantic Stratocumulus Transition Experiment (ASTEX). Our strategy is to focus on the vicinity of the cloud top using data collected from multiple cloud-top penetrations from the zigzag (or porpoising) legs. Using these measurements, we reveal inversion structure relative to the solid cloud top, the mixing in the entrainment zone (EZ), and the corrugated structure of the cloud top.

ASTEX was conducted during the summer of 1992 (1-28 June) off the northwest African coast, in the vicinity of the Azores and Madeira Islands. This region is dominated by intermittent low-level cloudiness with cloud conditions ranging from solid stratocumulus decks to broken trade cumuli. Randall (1995) gives a general overview of the project and Bretherton and Pincus (1995) particularly described the Lagrangian measurement strategy used during ASTEX where the aircraft followed an air column for continuous measurements. This study uses the measurements from three flights of the first Lagrangian measurements on June 12 and 13, 1992 (ASTEX flights 4, 5, and 6). The boundary layer structure and cloud evolution during these flights can be found in Bretherton and Pincus (1995).

Instrumentation for basic meteorological variables (wind turbulence, temperature, and humidity) on the NCAR Electra was described in many ASTEX-related papers (e.g., Wang and Lenschow 1995). Cloud droplet concentration was measured by a Particle Measurement System (PMS) Forward Scattering Spectrometer Probe (FSSP) using 15 channels between from 2 mm to 40 mm in droplet diameter. The cloud liquid water content used in this study was derived from the FSSP measurements.

2. THE ENTRAINMENT ZONE

During the ASTEX flight, porpoising legs across the cloud top were frequently made to sample the cloud top properties. Each of these short slant-path penetrations can be regard as a mini-sounding. Together, the multiple penetrations provide a spatially coherent view of the cloud top and the related thermodynamic and turbulence property. These porpoising legs are the main source of data for our analyses.

Figure 1 shows an example of one of the slant-path penetrations through the cloud top. All panels show the directly measured quantities except those with a prime (e.g., u') that show the perturbation variables. The perturbations were obtained using a wavelet filtering technique to remove the 'swings' or the sharp jumps in the measured quantity while focusing on the small-scale perturbations (Wang and Wang, 2004). Although the variations of all variables are shown with respect to height, it should be kept in mind that the aircraft went through a slant path. Hence what appears to be a vertical variation may in fact a presentation of the horizontal variations. For the measurements we analyzed here, the mean ascent/descent rate is about 3 m s^{-1}. The aircraft speed was about 100 m s^{-1}.

* *Corresponding author address:* Dr. Qing Wang, Naval Postgraduate School, Dept. of Meteorology, Monterey, CA 93940. e-mail: qwang@nps.edu

Figure 1 clearly shows a zone of strong variations in θ_v, q_v, and O_3 between 721 m and 736 m above sea level (ASL). This is the region of special concern in this paper. A few significant levels are worth noting in Fig. 1. For cloud, a maximum cloud liquid water of 0.3 g m^{-3} is seen at 715 m ASL, above which q_c decrease sharply. At 721 m height, q_c becomes 0.12 g m^{-3}. Although small, there are still signs of cloud water above (in both q_c and N_c) until 736 m. We refer to the layer between 721 m and 736 m as the wispy cloud layer due to the small amount of cloud water. The cloud with continuous sizable liquid water is referred to as solid cloud. The scalar variables also show distinctive properties in the different cloud layers. Below 721 m, θ_v, q_v, and O_3 show little perturbations (Figs 1i and 1j), which appears to be the undisturbed BL air. Significant perturbations of the scalar quantities are detected between 721 m and 736 m, corresponding to the wispy cloud layer. Here, we find pockets of BL air and the FA air, which is most evident in the specific humidity profile (Fig. 1c). The mixing analysis shown in the next section reveals that the layer also has mixtures of the BL air and the FA air. As a result, we refer to this layer as the entrainment zone (EZ). The EZ is best detected from the scalar perturbation plots (Figs. 1i and 1j) from the magnitude of perturbations in θ_v' and q_v'. The layer below the EZ will be referred to as the BL air.

Another significant feature in Fig. 1 is the presence of turbulence in the EZ. The profiles of the velocity components and their perturbations (Figs. 1e-1g, and 1l-1n), consistently depicts turbulence below 736 m ASL. However, we noticed larger magnitude of perturbations at the lower part of the sounding, clearly seen in the w perturbation profile. However, identifying a level above which turbulence becomes weaker is not always straightforward.

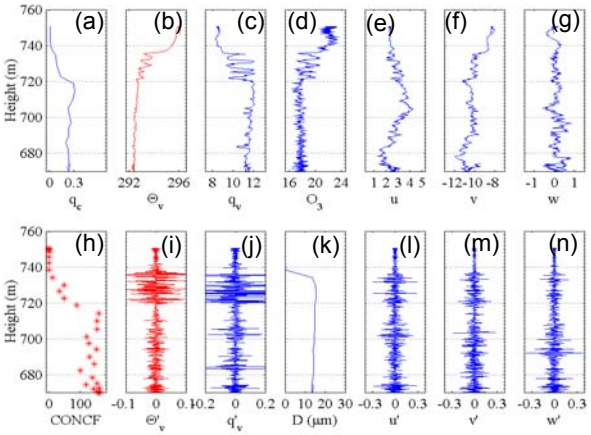

Figure 1. Vertical profiles from Research Flight 1, leg 1. (a) liquid water content (g kg^{-1}), (b) virtual potential temperature (K), (c) specific humidity of water vapor (g kg^{-1}), (d) ozone (ppbv), (e) u wind speed component (m s^{-1}), (f) v wind speed component (m s^{-1}), (g) w wind speed component (m s^{-1}), (h) cloud droplet concentration (N cm^{-3}), (i) θ_v perturbations, (j) q_v perturbations, (k) droplet size (μm) (l) u perturbations, (m) v perturbations, (n) w perturbations.

Figure 2 shows another example of the EZ seen in Fig. 1, but with some variations. In Figs. 2a and 2h, both q_c and N_c show continuous presence of cloud water below 740 m ASL, above which both drop to 0 within a few meters. A small wispy cloud is seen near 766 m below which there is a clear break above the solid cloud top. Since the aircraft sounding is not strictly vertical, the wispy cloud at 766 m is possibly a quick penetration through another cloud dome. At the same level of the solid cloud top, there is a sharp decrease of specific humidity (Fig. 2c). However, no temperature inversion was detected at the same level as oppose to the traditional view of the cloud top accompanied with a sharp inversion and a abrupt drop in water vapor. A weak inversion is detected at about 784 m (Fig. 2b), about 18 m above the cloud wisp at 766 m. Ozone concentration seems to change in concert with θ_v, where a gradual decrease is seen in the weak inversion (Fig. 2d). The three components of turbulence (u', v', and w') consistently show the change in turbulence perturbations from strong below the solid cloud top, to moderate in the layer between the cloud top and the inversion at 784 m, and to nearly no perturbations above the temperature inversion.

Clearly, Figs. 1 and 2 suggest a much more complicated cloud and thermodynamic structure in the vicinity of the cloud top that is different from the simple traditional view of sharp inversion at the cloud top and the non-turbulent air above. Here, the cloud top and the capping inversion are not necessarily collocated and there exist a thin layer between the two. Strong mixing of the inversion and boundary layer air is often seen in this layer as well as signatures of turbulence. These properties are consistent with entrainment mixing, which will be further illustrated in the next section.

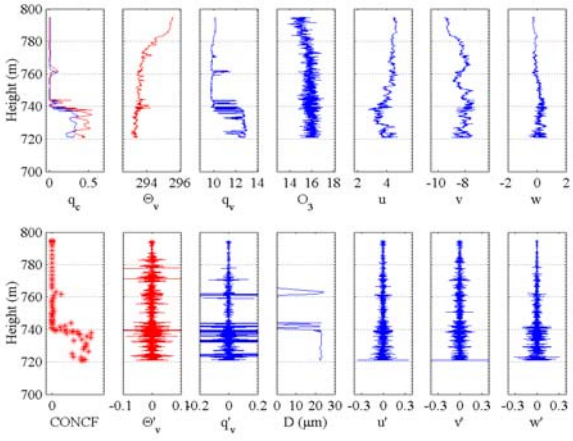

Figure 2. Same as in Fig. 1, except for sleg12 of Research Flight 5.

3. MIXING AND TURBULENCE IN THE ENTRAINMENT ZONE

In this section, we will illustrate the characteristics of mixing and turbulence in the entrainment zone. Figure 3 is another example of entrainment mixing from Flight 6 of ASTEX. The entrainment zone in this sounding is approximately 38 m deep, from 905 to 943 m. Within this layer, significant and strongly correlated variations of cloud water, temperature, water vapor, and ozone are clearly seen, suggesting undiluted pockets of FA and the BL air. The vertical extent of the pockets is about 1 to 5 m. Given the aircraft horizontal speed of 100 m s^{-1}, the depth of the FA and BL air pockets correspond to a horizontal distance of 100 to 500 m. Drier and warmer pocket corresponds the few or no cloud water while q_c is detected in most pockets with cool and moist air.

Mixing-line analyses were performed to further analyze the mixing properties in the entrainment zone (Fig. 4a). The blue circles on Fig. 4a are from below the EZ representing the boundary-layer air, the smaller red circles on the right-hand side of the diagram represent the FA air. The green dots in-between are those from the entrainment zone. The connected circles represent the mixture at mixing fractions (ratio between the mass of the FA air to that of the mixed parcel) from 0 (totally BL air) to 1 (totally FA air) at 0.1 increments. The probability distribution of the mixing fraction from the same sounding (Fig. 4b) shows that the air in the EZ is predominantly BL air.

The result on the mixing fraction in the EZ in Fig. 4b is not representative of others. Another sounding, approximately 40 km downstream from that in Fig. 3 shows an EZ of 25 m deep that contains mostly FA and much weaker turbulence compared to the layer below. Upon further inspection of other soundings, we found that the probability distribution of the mixing fraction in the EZ can take on any form. It became evident that the strength of turbulence in the entrainment zone has to do with the distribution of the mixing fraction. When BL air dominates the EZ, turbulence in the EZ is similar to that below the solid cloud top. No or very weak turbulence is often associated with the large amount of FA air in the EZ. The amount of cloud water in the EZ is also connected with the amount of BL air. The connections between the strength of turbulence and the cloud water amount with the mixing fraction suggest the intermittent nature of entrainment mixing. The variety of distribution of mixing fraction in the EZ suggests a time sequence of entrainment mixing, the greater the lapse in time from the start of entrainment mixing, the greater the probability that air in the EZ will have the characteristics of FA air accompanied with less cloud and weaker turbulence in the EZ. The soundings indicate that the detected local entrainment mixing tends to evaporate the cloud in the entrainment zone.

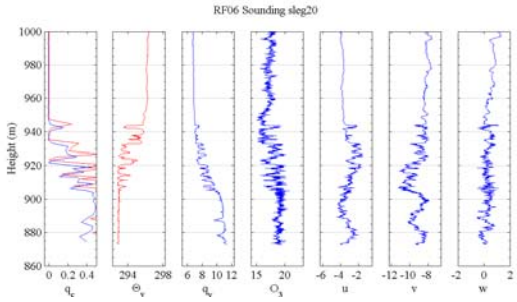

Figure 3. Same as in Fig. 1a - 1g, except for Research Flight 6, leg 20.

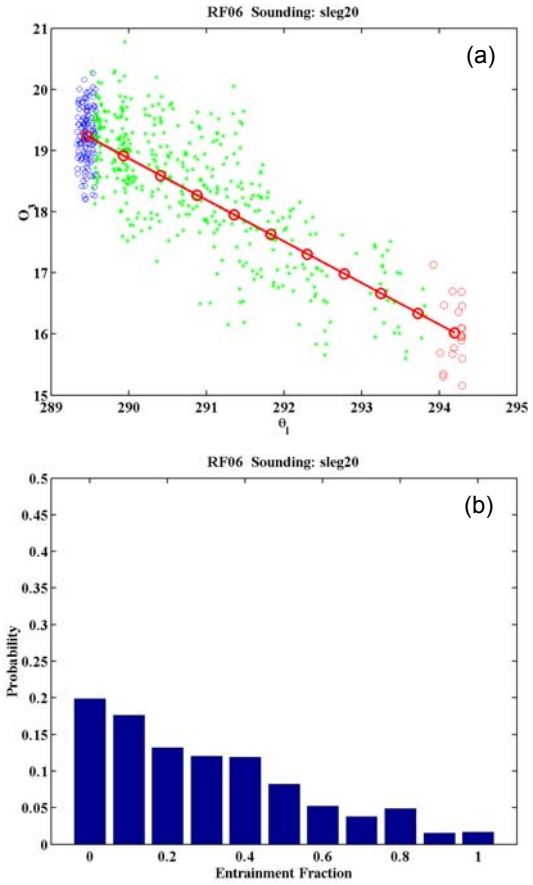

Figure 4. (a) Mixing line analysis for Research Flight 6, leg 20. (b) Probability histogram for Research Flight 6, leg 20.

4. ENTRAINMENT ZONE DEPTH

To better characterize the entrainment zone, we analyzed 105 soundings from three Lagrangian flights

during ASTEX. These three flights were chosen because they cover a large range of boundary layer depth. The general meteorological condition, cloud evolution, and turbulence were documented well by previous studies (e.g., Bretherton and Pincus, 1995). For each sounding, we identify the heights of the entrainment zone base (z_{ezb}), the entrainment zone top (z_{ezt}) from the profiles of scalar variables and their perturbations (indication of mixing). z_{ezb} is defined by visual inspection of the temperature and humidity being consistent with the BL air. In many cases, z_{ezb} is also the lowest height of strong scalar perturbations. z_{ezt} is the highest level of strong perturbations of $\theta_v^{'}$ and $q_v^{'}$. We also identify the heights where strong turbulence ends (z_{st}), and the height where weak turbulence ends (z_{wt}) whenever the difference in turbulence perturbations between the upper and the lower BL are detectable. In cases when changes in turbulence strength are not obvious, the height where turbulence ends is assigned as z_{st} and no z_{wt} is defined.

Figure 5 shows the relationship among these significant heights. We found that z_{st} correlates well with z_{ezb} as expected of the turbulent boundary layer (not shown). On the other hand, z_{wt} corresponds well with z_{ezt}, and when present, is always higher than z_{ezb}. While the majority of the entrainment zone show some signs of cloud water, the solid cloud top in most of the soundings appear to coincide with z_{ezb} (Fig. 5b). The difference between z_{ezb} and z_{ezt} gives the depth of the EZ and averages to 16.4 m from the three flights.

5. ENTRAINMENT AND THE CORRUGATED CLOUD TOP

The multiple penetrations through the cloud top from the porpoising legs provided a vertical cross section of cloud and boundary layer properties. This allowed for a spatially coherent view of the cloud top and the EZ. An example of the cloud-top structure obtained from one of the porpoising legs in Flight 5 is given in Fig. 6. This type of imagery has not appeared in previous literature for stratocumulus-topped boundary layers.

The dominant feature of the cloud top is an undulating surface that oscillates as a series of troughs and ridges. Figure 5 shows the depths of the cloud-top

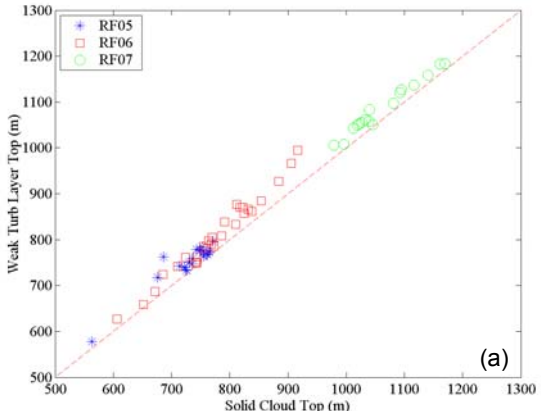

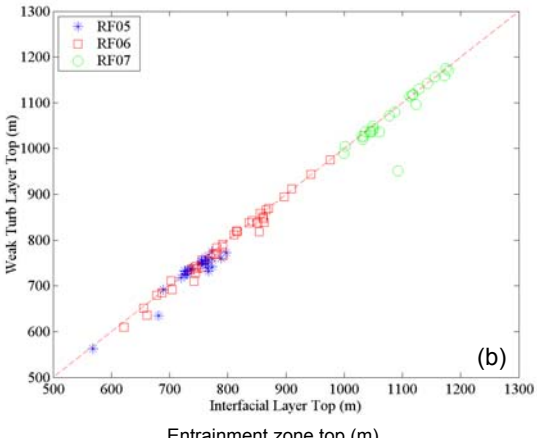

Figure 5. A scatter-plot diagram of (a) z_{st} vs z_{ezb}; (b) z_{wt} vs. z_{ezt}. Data is from all soundings of the first Lagrangian IOP of ASTEX.

ridges and troughs are on the order of 10 to 20 m. The width of these features is on the order of 5 to 10 km. Corresponding to each cloud ridge, there appears to be a local maximum of liquid water content. Wispy cloud patches above the solid cloud top are best detected above the cloud ridges (*e.g.*, at about 3 and 26 km into the flight track). We note that the air immediately above the troughs of the solid cloud-top contains cloud droplets as well, although the cloud water is normally small.

In order to view the spatial variation of other variables relative to the cloud top, cloud boundaries are denoted in Fig. 6. Here, we use the highest level where q_c approaches 0.04 g Kg^{-1} as the top of the cloud (top of the wispy cloud when present). The solid cloud top is taken as the lowest level above the peak q_c where q_c reaches 0.12 g Kg^{-1}. The value of 0.04 g Kg^{-1} as the

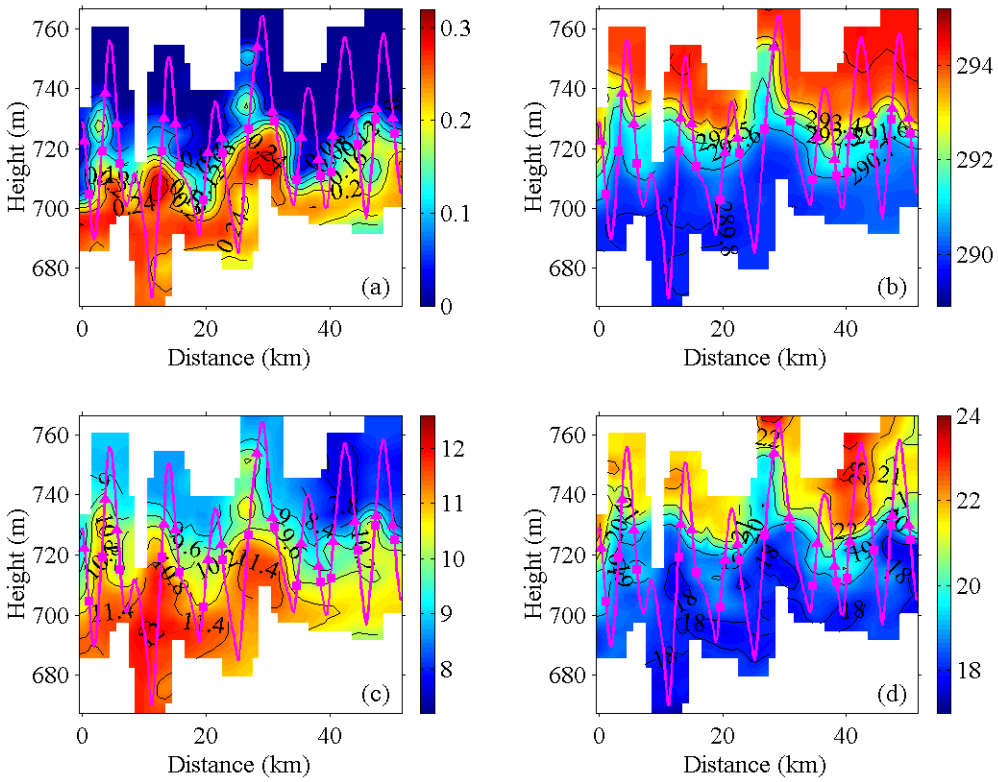

Figure 6. Vertical cross section of (a) liquid water content; (b) liquid water potential temperature; (c) total water specific humidity; and (d) ozone concentration from one of the zigzag soundings during Research Flight 5 of ASTEX. The measurements from the FSSP-100 Cloud Probe were used in this plot. The thin magenta line denotes the flight track. The horizontal axis represents the distance from the starting point of the flight leg. The 'Δ' and '□' denote the height at which cloud liquid water content are 0.04 and 0.12 g Kg^{-1}, respectively.

cloud boundaries were also used by Lenschow et al. (2000) with aircraft measurements. The threshold of 0.12 g Kg^{-1} is picked from our experience inspecting through many soundings in ASTEX. In general, above the level of 0.12 g Kg^{-1} in q_c, strong inhomogeneous mixing with the inversion air can be detected. These cloud boundaries are denoted as 'Δ' and '□' in Fig. 6. When these two cloud boundaries are close (*e.g.*, within several meters), it depicts a solid cloud top with no sizable wispy cloud layer above.

Fig. 6b shows the persistent presence of an inversion seen in liquid water potential temperature (θ_l). However, the height of the inversion tends to follow that of the wispy cloud top when it exists even though in some cases the cloud water in the wispy cloud layer are hardly detectable. Thus in case of a deep local EZ (such as at 3 and 26 km into the flight track in Fig. 5a), the strongest inversion is usually not at the immediate solid cloud top. This is consistent with what we see from a single sounding discussed in Section 2. Nevertheless, the air between the two cloud boundaries is generally high in θ_l compared to the boundary layer air, which indicates that entrainment mixing had occurred. Variation of the ozone concentration across the cloud top is similar to θ_l with the largest gradient seen at the wispy cloud top. Ozone in the wispy cloud is in general the same as below the solid cloud, suggesting that the wispy cloud layer was, and may still is, part of the boundary layer.

The total water specific humidity (q_T, Fig. 6c) observed in ASTEX perhaps represents the largest deviation from the traditional view of a cloudy boundary layer capped by strong inversion and sharp decrease in total water. Frequently, significant gradient of total water is observed in the EZ (Fig. 6c), below the sharp inversion. Figure 6c also shows that the start of the total water gradient coincides with the solid cloud top. However, spikes of dry air are frequently observed from the sounding profiles. In Fig. 1c we find a dry pocket of 2 m deep at 684 m where q_v decreased from the 11.5 g kg^{-1} BL value to 10.5 g kg^{-1}. Another example is seen in

Fig. 3 at 888 m and 878 m, where O_3 also show slight decreases. Corresponding to these dry pockets, we also observed decreases of cloud water (Figs. 1a and 3a). However, unlike in the EZ zone, the pockets do not show perturbations in θ_v. Entrained dry and cool parcels were observed in the main body of the boundary layer (in the lower cloud layer and below) associated with buoyancy reversal effect of entrainment (Wang and Albrecht 1994). These dry pockets are the same penetrating entrainment event. These perturbations cannot be revealed from the contour plots using the porpoising legs because they are smaller than the vertical resolution used to generate the plots.

6. DISCUSSIONS

In this study, we have revealed the fine structure of the EZ using multiple penetrations through the cloud top. The profiles are in fact from slant path aircraft soundings, which strictly speaking, are not exactly vertical variations. Most of the soundings in ASTEX were made at an ascent/descend rate of about 3 m s^{-1} (500 ft min^{-1}). Given the aircraft speed of about 100 m s^{-1}, the mean slope of the slant path is about 0.03. Hence, what is depicted as vertical variation in the profiles is in fact a combination of horizontal and vertical variations.

To understand what we have seen from the slant path soundings, we analyzed the variation of the cloud top using lidar measurements of the cloud top from the First ISCCP Regional Experiment (FIRE-I) conducted during June/July of 1987 off the coast of southern California (lidar measured cloud-top height is not available for ASTEX). We found that the corrugated cloud top varies significantly from several tens of meters to kilometers. The amplitude of the small-scale variation is on the order of 10-20 m, while the kilometer-scale variations can vary by as large as several hundred meters. In a recent study by Gerber et al. (2005), they found pockets of depleted liquid water contents (cloud holes) of several meters in width. To ascent/descent through the entrainment zone of 16 m in depth, the aircraft may go through several cloud wisps along the flight path. Hence, the wispy cloud water content in the sounding is likely from different horizontal location within several hundred meters in distance. The entrainment zone defined in this study is therefore not the depth above the local cloud top where entrainment mixing occurs, it should be taken, in a statistical sense, the depth above the mean solid cloud top where entrainment mixing occurs.

Given the spatial resolution of the soundings in each porpoising leg, the cloud structure and the horizontal variation thermodynamic quantities in the EZ (Fig. 6) are equivalently a horizontally filtered view with a filter length of several kilometers. The slant path effect is, however, factored in as horizontal coverage of the soundings are considered in generating the contour plots.

7. ACKNOWLEDGEMENTS

This research is sponsored by Office of Naval Research.

8. REFERENCES

Bretherton, C. S., and R. Pincus, 1995: Cloudiness and marine boundary layer dynamics in the ASTEX lagrangian experiments. Part I: Synoptic setting and vertical structure. J. Atmos. Sci., 16, 2707-2723.

Gerber, H., G. F. ans S. P. Malinowski, S. L. Brenguier, and F. Burnet, 2005: Holes and entrainment in stratocumulus. J. Atmos. Sci., 62, 443-459.

Lenschow, D. H., M. Y. Zhou, X. B. Zeng, L. S. Chen, and X. D. Xu, 2000: Measurements of fine-scale structure at the top of marine stratocumulus. Boundary-Layer Meteorol., 97,331-357.

Lilly, D., 1968: Models of cloud-topped mixed layers under a strong inversion. Q. J. R. Meteorol. Soc., 94, 292-309.

Moeng, C. H., B. Stevens, and P. P. Sullivan, 2005: Where is the interface of the stratocumulus-topped PBL? J. Atmos. Sci., 62, 2626-2631.

Nicholls, S., and J.D. Turton, 1986: An observational study of the structure of stratiform cloud sheets: Part II. Entrainment. Quart. J. R. Met. Soc., 112, 461-480.

Randall, D. A., 1995: Editorial, Atlantic stratocumulus transition experiment. *J. Atmos. Sci*., **16**, 2705.

Wang, Q., and D. H. Lenschow, 1995: An observational study of the role of penetrating cumulus in a marine stratocumulus-topped boundary layer. J. Atmos. Sci., 16, 2778-2787.